Inverted fireball deposition of carbon films with extremely low surface roughness

Article *in* Carbon Letters · October 2022

DOI: 10.1007/s42823-022-00424-9

8 authors, including:

Johannes Gruenwald
Gruenwald Laboratories GmbH
57 PUBLICATIONS **394** CITATIONS

SEE PROFILE

Carbon Letters
https://doi.org/10.1007/s42823-022-00424-9

Online ISSN 2233-4998
Print ISSN 1976-4251

ORIGINAL ARTICLE

Inverted fireball deposition of carbon films with extremely low surface roughness

J. Gruenwald[1] · G. Eichenhofer[2] · G. Filipič[3] · Ž. Federl[3] · W. Feuchtenberger[5] · K. Panos[5] · G. Hernández Rodríguez[4] · A. M. Coclite[4]

Received: 1 August 2022 / Revised: 26 September 2022 / Accepted: 10 October 2022

Abstract
The surface of carbon films deposited with inverted plasma fireballs is analysed in this paper. Measurements were conducted with Raman spectroscopy, atomic force microscopy and nanoindentation. The latter was used to obtain Young's modulus as well as Martens and Vickers hardness. The roughness of the film was measured by atomic force microscopy and its thickness was measured. It was shown with Raman spectroscopy that the films are homogeneous in terms of atomic composition and layer thickness over an area of about 125 × 125 mm. Furthermore, it was demonstrated that inverted plasma fireballs are a viable tool for obtaining homogeneous, large area carbon films with rapid growth and very little energy consumption. The obtained films show very low roughness.

Keywords PECVD · Carbon · Inverted fireballs · Deposition

1 Introduction

Various carbon containing films, ranging from graphene over amorphous carbon and nanostructured surfaces to diamond like carbon layers have gained more and more momentum in recent years. This is mostly due to their vast number of properties that can be tailored by fine tuning the kind of carbon allotrope deposited onto different substrates. Amongst many possible technologies for carbon film deposition, plasma enhanced chemical vapour deposition (PECVD) is a standard procedure. It has successfully been used to obtain carbon nano structures [1, 2], graphene [3, 4], diamond like carbon (DLC) [5, 6], diamond [7, 8] or amorphous carbon films [9, 10]. In recent years, a novel PECVD process, which is based on so-called inverted fireballs (IFBs) has gained increased attention, since it allows the creation of very homogeneous plasmas with enhanced plasma densities [11–15]. There have also been attempts to incorporate an IFB setup into a sputter chamber but so far with mixed results [16]. The favourable combination of high plasma density and homogeneity is obtained by a highly transparent grid that is put onto a suitable positive potential with respect to ground. If the bias becomes larger than the ionisation potential of the working gas, electrons are attracted from the surrounding background plasma and accelerated towards the gridded anode. Most of these highly energetic electrons will pass through the grid and induce additional ionisation processes in the closed wire cage. At the same time, the Debye sheath around the mesh wires overlaps with the sheath of the neighbouring wires and, thus, forms an equipotential surface around the entire gridded anode. This leads to a formation of a Faraday cage, in which the denser plasma is trapped and forms the IFB. While the ions are trapped in the potential well that forms inside the mesh cage, electrons can escape through the grid or passing between two opposite sides of the cage. If this happens, the escaping electrons are influenced by the electric field of the mesh as soon as they leave the IFB. This field accelerates them back into the IFB, artificially prolonging

✉ J. Gruenwald
jgruenwald@g-labs.eu

1 Gruenwald Laboratories GmbH, Taxberg 50, 5660 Taxenbach, Austria

2 4A-PLASMA, Aichtalstraße 66, 71088 Holzgerlingen, Germany

3 Jozef Stefan Institute, Jamova Cesta 39, 1000 Ljubljana, Slovenia

4 Institut Für Festkörperphysik, Graz University of Technology, NAWI Graz, Petersgasse 16, 8010 Graz, Austria

5 Institut Für Elektronik Und Messtechnik, Helmut Fischer GmbH, Industriestraße 21, 71069 Sindelfingen, Germany

Published online: 18 October 2022

their collision mean free path and enhancing their kinetic energy. Therefore, those electrons trigger additional ionising collisions within the IFB, enhancing the plasma density by up to an order of magnitude. Although the plasma potential is essentially flat throughout an IFB, it was experimentally demonstrated in reference [15] that the potential profile can be tailored to a certain extent, if one or more sides of the cage are electrically insulated against the others and biassed slightly different than the main cage anode [15]. This may be used in setups where a gradient in the plasma potential and, hence, in the difference of ion and electron densities is desirable. IFBs are a novel technology, which offers the possibility of homogeneous depositions over large areas. Furthermore, the growth rates are quite high even with low additional power consumption by the IFB electrode. Nevertheless, the focus of this paper lies on a standard IFB in a mixture of argon and n-hexane and the films that were deposited with this method. After the successful deposition of the carbon films, the physical properties of the layers were studied with different methods, which will be discussed in detail in the next section.

2 Materials and methods

The carbon films were deposited in a vacuum chamber, type PA 100 from Plasma Technology GmbH at a working pressure of 3 Pa. The chamber was evacuated by a turbo pump. The background plasma was maintained at 40 kHz, 50 W. For applying the DC Voltage to the grid, a power supply from EDF electronics was used. The IFB anode was manufactured from a stainless steel grid with (wire diameter 120 µm, grid constant 250 µm). It had a height of 8.5 cm and an edge length of 18.5 cm and consumed 20 W of electrical power at a voltage of 174 V. The substrate was not additionally heated and remained at room temperature due to the little overall power. The IFB setup and the plasma parameters are shown in detail in reference [17]. A schematic diagram of the electrical setup of the IFB cage is shown in Fig. 1.

The deposition was conducted on standard laboratory soda-lime glass slides (as used for microscopy) with 25×75 mm^2 area. 7 of these glass plates were covering the substrate holder. An additional slide was put on top of the others to cover the glass substrate and have a reference of uncovered glass samples after the deposition. Before the coating process an IFB was ignited in a mixture of 100 sccm H_2 and 7.5 sccm Ar to clean the substrates. This cleaning process was upheld for 5 min. After the initial cleaning, a second IFB plasma was ignited in a mixture of 50 sccm Ar and 50 sccm tetramethylsilane (TMS) for 1 min to obtain an adhesive mediation layer between the glass substrate and the carbon film. After this, the coating process was conducted in an Ar/n-hexane IFB (with 100 sccm each) for 15 min. The result of this coating experiment is depicted in Fig. 2.

It is evident that a smooth carbon containing film was obtained within the IFB grid. After the coating procedure,

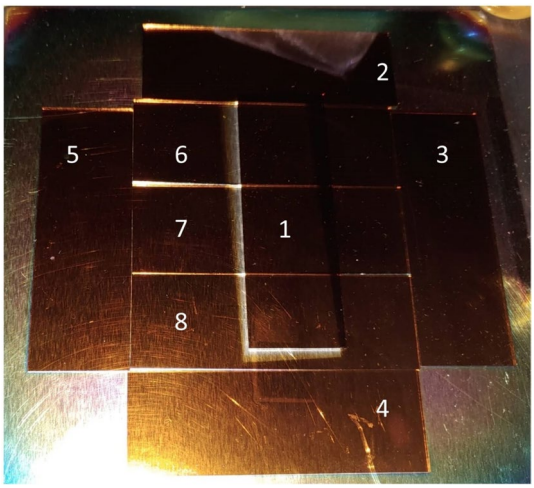

Fig. 2 Samples after 15 min of IFB deposition. The substrates 1–8 were glass slides with 25×75 mm^2 area. The slight dislocation of slide one was due to mechanical vibrations that occurred when opening the chamber

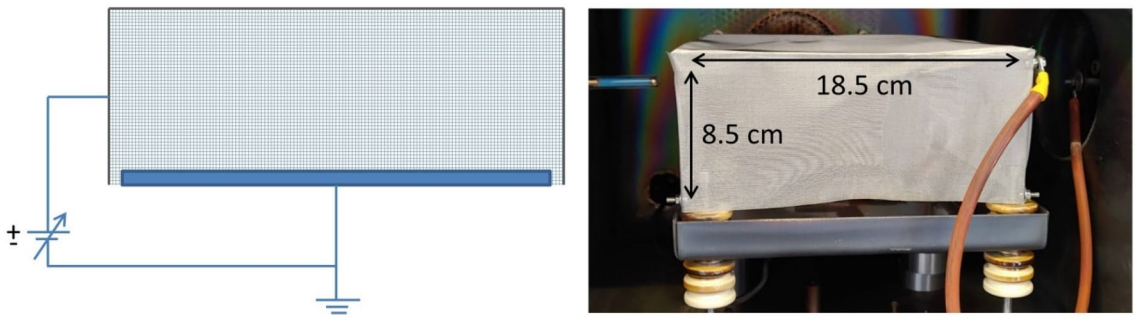

Fig. 1 Schematic diagram of the IFB setup with electrical connections (left) and a photograph of the anode grid on top of the substrate holder (right, taken from reference [17].)

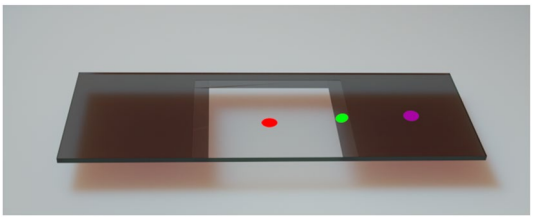

Fig. 3 The points of measurements for the Raman and AFM data acquisition

the samples were analysed with different methods that are outlined in the next section.

3 Results

3.1 Raman measurements

Raman spectroscopy was performed on the two different areas, shown in Fig. 3. On the uncoated glass sample (red dot) and the carbon film itself (pink dot). The transition region (green dot) was also investigated with AFM. These results will be presented below. The samples were analysed with a Witec Raman spectroscope using a green laser with 532 nm and 4 mW output power on the glass substrate to get Raman peaks with reasonable intensity. However, the power of the laser was reduced to 1.6 mW on the carbon films to prevent possible damages. This is still enough due to the increased Raman sensitivity of carbon films.

Each sample was measured at least at two points in each of the relevant regions—glass and carbon. The obtained data are displayed in Fig. 4. Since the most interesting region is the carbon film, Fig. 4b depicts the collected data from random samples (2, 3, 4 and 8 in this case) to illustrate that the Raman peaks are indeed identical, regardless of the substrate's position within the IFB.

The peaks in Fig. 4a can be identified as the symmetry stretching mode of Si–O bonds from the glass slide (570 cm^{-1}) [18], a high frequency Si–O-Si binding mode (794 cm^{-1}) [19] and the so-called Q^3 Si–O stretching vibration mode (1098 cm^{-1}) [20]. With increasing thickness, the Raman peaks from the glass substrate are vanishing and only one broad peak remains. This peak was deconvoluted into two separate peaks at 1383 cm^{-1} and 1546 cm^{-1}, respectively. The former is as assumed to be the stretching mode of the CH_3 alkyl group while the latter is attributed to the aromatic Si–C vibration mode [21]. Since the peak position and intensities are identical on all the measured samples, it can be concluded that the

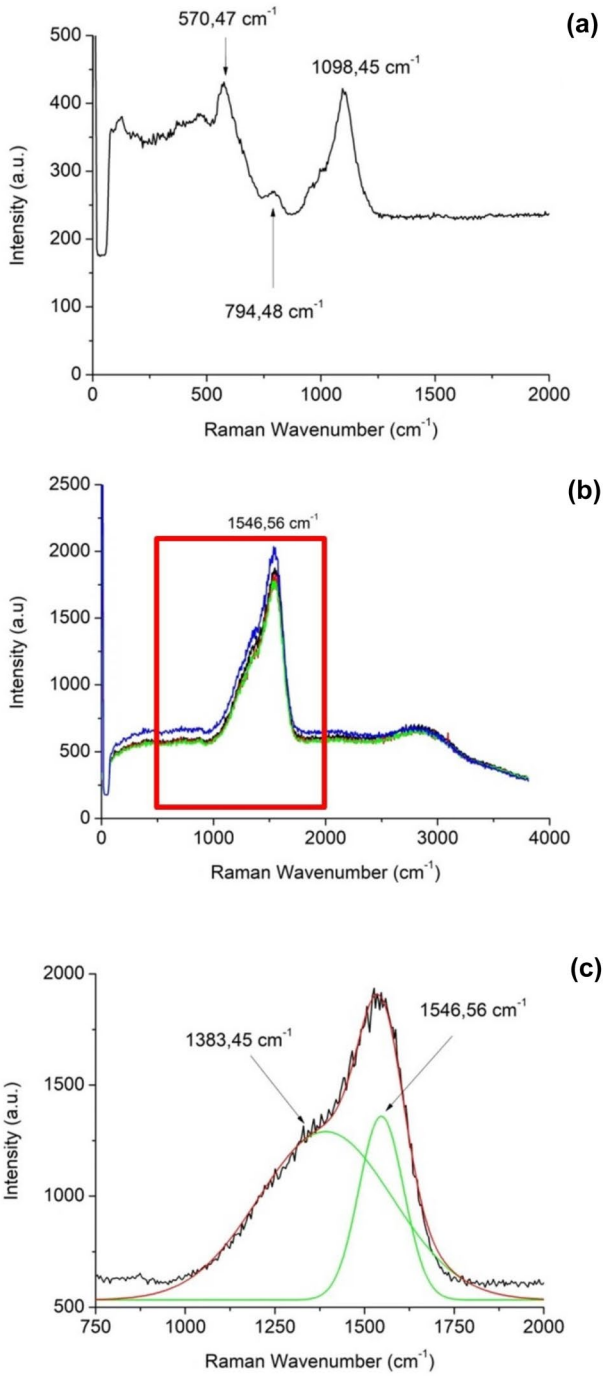

Fig. 4 Raman spectra of the glass substrate **a** and the carbon film (**b**). Image **c** shows a magnified view of the deconvoluted peak at 1546 cm^{-1}

chemical composition of the films is very homogeneous throughout the entire substrate and, thus, throughout the entire plasma inside the IFB. This assumption is also corroborated by the measurements in reference [17].

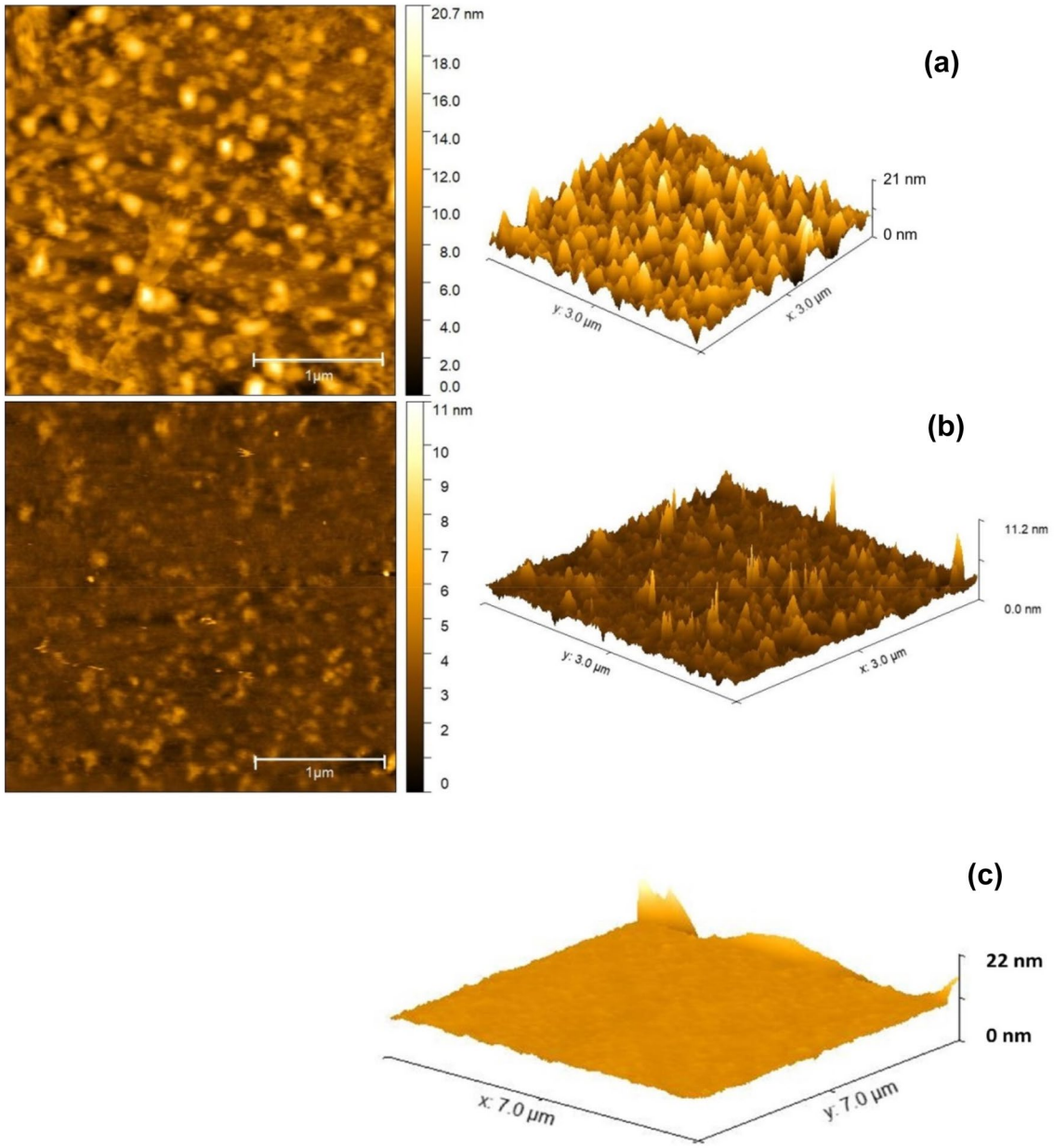

Fig. 5 AFM images and surface map of the glass substrate (**a**), the transition region (**b**) and the carbon film (**c**)

3.2 AFM measurements

To study the surface morphology, AFM measurements were performed on the glass and on the carbon coating. The results are shown in Fig. 5.

The uncoated glass as well as the transition region was analysed on a 3×3 µm^2 area while the carbon coating was investigated on a 7×7 µm^2 area. It can be seen that the highest elevation on the surface is about 22 nm with rms roughness of 2.349 nm, while the rms roughness on the transition region decreases down to 0.553 nm with the highest elevations at around 11 nm. However, on the carbon coating the roughness decreases further below the resolution of the AFM (< 0.25 nm). Approaching the resolution limit of the AFM also causes the artefact at the end of the measurement in Fig. 5c. The same results were obtained on all the samples, indicating again that the morphology of the carbon layer produced with IFB shows a very smooth and homogeneous surface throughout the whole IFB plasma region.

3.3 Nanoindentation measurements

Nanoindention or instrumented indentation testing was performed according to DIN EN ISO 14577, which provides

access to information about the mechanical properties of the obtained films. The used instrument in these experiments was a PICODENTOR HM 500 from the Helmut Fischer GmbH with a Vickers indenter. A maximum force of 100 µN was used as parameter for the standard measurement procedure. The loading and unloading of the force occurred within 3 s. In addition, an enhanced stiffness procedure (ESP) with a maximum force of 100 mN applied during 912 s was utilised to gain further depth-dependent information. The measured indentation depth h as a function of the applied force F is depicted in Fig. 6.

The Martens hardness (HM) was calculated from the load curve and is shown as a function of depth in Fig. 7.

While the HIT value can be converted into the Vickers hardness (HV), the elastic properties have been calculated from the unloading of the lever in accordance with the method proposed by Oliver and Pharr [22]. This method yields the so-called indentation modulus EIT.

The force-penetration depth curves (Fig. 6) point out that the deposited layer exhibits a considerable difference in mechanical properties compared to the glass substrate. The increase in the curve fraction of the loading demonstrates a clear difference. Furthermore, the maximum penetration depth in the coating is higher than in the glass substrate. It is therefore evident that the coating must have a lower hardness. This was confirmed by the hardness parameter HM in Fig. 7. The graph shows that the hardness of the coating is not only lower, but also shows a stable or homogeneous behaviour in depth without any hardness gradient.

Other commonly used hardness properties determined for the coating, that cannot be represented as a function of depth in a standard measuring procedure, are HIT of 8.8 GPa ± 0.07 GPa and the Vickers hardness value of 827 HV ± 7 HV.

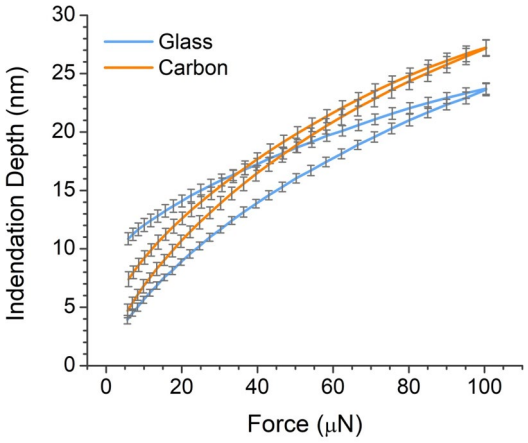

Fig. 6 Averaged indentation depth h as a function of the applied force F

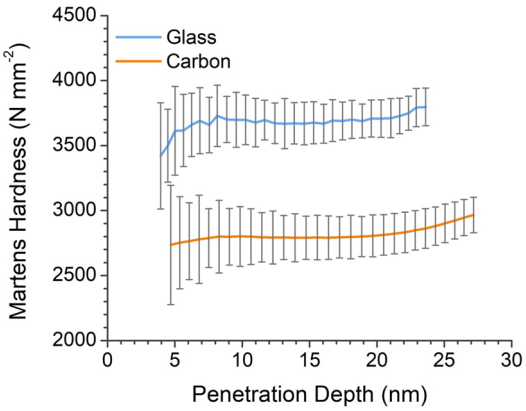

Fig. 7 Depth dependent Martens hardness (HM) as a function of the penetration depth

In addition to the hardness properties, the elastic properties were also determined using the characteristic value EIT/(1-νs^2). The mentioned parameter approximately characterises the elastic modulus of the coating, without considering the Poisson's ratio (νs). Based on these measurements, an EIT/(1-νs^2) of 70.7 GPa ± 2.6 GPa was determined for the glass and 47.9 GPa ± 0.3 GPa for the coating.

When comparing the measurements from the standard measurement procedures with those from the ESP in Fig. 8, it is clearly evident that this allows an estimation of the layer thickness. The previously determined characteristic values from the standard measurement procedure can be seen again within the measurement uncertainty. Only the characteristic values EIT/(1-νs^2) and HM were shown for clarity.

For both considered characteristic values, a comparable measured value from the standard procedure can be determined from the diagram in Fig. 8. The special feature here is that a significantly greater penetration depth was run. This means that, according to the 10% rule, the properties of the coating are represented by only one point at approx. 28 nm.

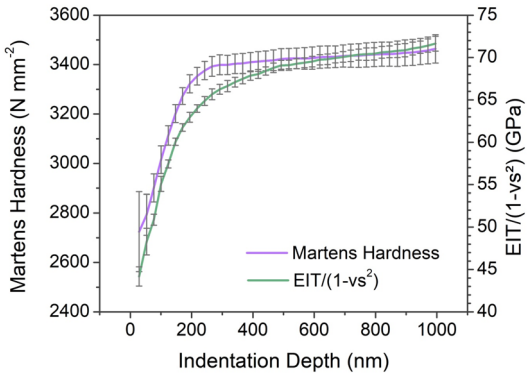

Fig. 8 Averaged depth-dependent characteristic value of HM and EIT/(1-νs^2), measured with ESP

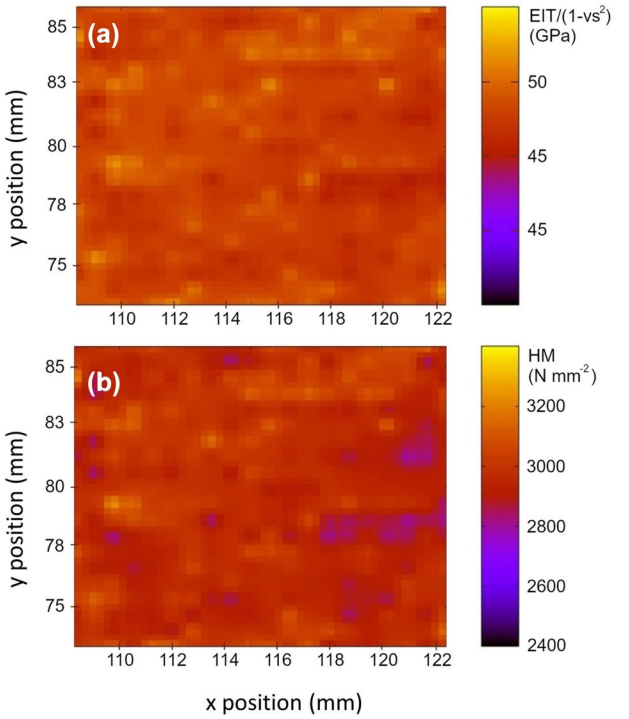

Fig. 9 Colour-coded plot of EIT/(1-νs^2) (**a**) and HM (**b**) for testing the layer homogeneity

The hardness value is influenced by the substrate material at greater depths. This can also be seen in the elastic behaviour, so that two curve components with different slopes can be distinguished. At the turning point of the slopes, a layer thickness can be estimated, which can be assumed to be approx. 200–300 nm.

For the analysis of the layer homogeneity, an array of measuring points was taken on a sample with the nanoindentation instrument. A matrix with a measurement area of 12.65 mm by 14.2 mm was applied to the sample to obtain an impression of the homogeneity.

The 341 measurement curves obtained in this area were used to generate a colour-coded plot of various properties of the measurement matrix, which can be seen in Fig. 9.

The thin layer exhibits a satisfactory homogeneity over the measured sample area in terms of hardness and Young's modulus, which can be seen from HM and EIT/(1- νs^2). No gradients of the considered properties over a large area of the sample can be seen. The results are statistically normal-distributed. This allows the conclusion that a homogeneous deposition result was obtained in the process.

3.4 Measurements of the film thickness

The evaluation of the coating thickness was also performed by Helmut Fischer GmbH. These measurements were conducted with a BETASCOPE using a radioactive source C14 at a temperature of 22 °C with a measuring time of 100 s. We measured a mean value of 263 nm and a standard deviation of 50 nm for the coating thickness by assuming 1.395 g/cm^3 for the density of the coating.

Table 1 Results and statistical parameters of the mechanical properties of the carbon films and maximum indentation depth h_{max}

	HM N/mm^2	EIT/(1-νs^2) GPa	HIT N/mm^2	HV	h_{max} nm
X	2966	47.9	8752	827	27
U (X.)	14	0.25	65	7	0.1
S	137	2.4	608	58	0.7
V/%	4.6	4.9	7	7	2,6
Min	2658	42.3	7148	675	25
Max	3451	55.2	11060	1045	29

4 Conclusions

In this paper, the deposition of large area amorphous carbon coatings with excellent homogeneity by applying IFBs is reported. The measurements of the mechanical and surface properties showed that films with low surface roughness and homogeneous chemical composition were obtained with growth rates of about 15–20 nm/min at very low overall input power (approx. 70 W). The coating experiments demonstrate that IFBs are a versatile tool, especially for the fabrication of large area carbon films, which demand a small surface roughness and high level of homogeneity. An overview of the results from the mechanical analysis and the relevant statistical parameters from these measurements are listed in Table 1.

The main purpose of this paper is to show that IFB can produce carbon layers with relevant properties. However, there will be more work necessary in the future regarding suitable precursor gases or gas mixtures and the fine tuning of other physical parameters such substrate temperature, gas pressure, et cetera which are expected to enhance the number of varieties for other carbon allotropes on different substrate materials.

Acknowlegdements The authors want to thank J. Eisenlohr from Plasma Technology GmbH, 71083 Herrenberg-Gültstein, Germany for the making the PA 100 plasma system available for the experiments and his technical support. J. Gruenwald: Member of the GET-Plasma Consortium, G. Eichenhofer: Member of the GET-Plasma Consortium.

Declarations

The authors declare that they have no conflicts of interest.

References

1. Neyts EC (2012) PECVD growth of carbon nanotubes: from experiment to simulation. J Vac Sci Technol, B: Nanotechnol Microelectron: Mater, Process, Meas, Phenom 30(3):030803
2. Santhosh NM et al (2020) Oriented carbon nanostructures from plasma reformed resorcinol-formaldehyde polymer gels for gas sensor applications. Nanomaterials 10(9):1704
3. Guo L et al (2018) Direct formation of wafer-scale single-layer graphene films on the rough surface substrate by PECVD. Carbon 129:456–461
4. Hussain S et al (2020) Low-temperature low-power PECVD synthesis of vertically aligned graphene. Nanotechnology 31(39):395604
5. Wei X et al (2021) Deposition of DLC films on the inner wall of U-type pipes by hollow cathode PECVD. Diam Relat Mater 114:108308
6. Mayer M et al (2016) Diamond like carbon deposition by inverted fireballs. Materials Today: Proceedings 3:S184–S189
7. Mesbahi A, Silva F (2017) Study of the influence of gas flow on PECVD diamond growth: influence of the separate injection of gases. J Phys D Appl Phys 50(47):475203
8. Taylor A et al (2022) Growth and comparison of high-quality MW-PECVD grown B doped diamond layers on 118}, {115 and 113 single crystal diamond substrates. Diam Relat Mater 123:108815
9. Sheng R et al (2018) Effect of unbonded hydrogen on amorphous carbon film deposited by PECVD with annealing treatment. Diam Relat Mater 81:146–153
10. Cho Y-S et al (2019) Effect of substrate bias on biocompatibility of amorphous carbon coatings deposited on Ti6Al4V by PECVD. Surf Coat Technol 357:212–217
11. Gruenwald, J., et al. (2011) "Further experiments on inverted fireballs." Proc. 38th EPS Conf. Plasma Phys, 2011.
12. Gruenwald J, Reynvaan J, Knoll P (2014) Creation and characterization of inverted fireballs in H2 plasma. Phys Scr 2014(T161):014006
13. Knoll P et al (2016) PECVD of carbon by inverted fireballs: from sputtering, bias enhanced nucleation to deposition. Diam Relat Mater 65:96–104
14. Gruenwald J, Reynvaan J, Geistlinger P (2018) Basic plasma parameters and physical properties of inverted He fireballs. Plasma Sources Sci Technol 27(1):015008
15. Gruenwald J, Reynvaan J, Geistlinger P (2020) Influence of inhomogeneous electrode biasing on the plasma parameters of inverted H2 fireballs. J Technol Sp Plasmas 1(1):1–4
16. Gruenwald J et al (2021) Application and limitations of inverted fireballs in a magnetron sputter device. Surf Coat Technol 422:127510
17. Eichenhofer G et al (2022) Measurement of inverted n-hexane fireball properties with a Multipole Resonance Probe. J Technol Sp Plasmas 3(1):109–117
18. Duan R-G, Kai-Ming L, Shou-Ren G (1998) Effect of Na+ ion on the structure of 27CaO· 12Al2O3· 61SiO2 glass. Mater Chem Phys 57(1):92–94
19. Henderson GS et al (1985) Raman spectra of gallium and germanium substituted silicate glasses: variations in intermediate range order. Am Miner 70(9–10):946–960
20. O'Shaughnessy C et al (2020) The influence of modifier cations on the Raman stretching modes of Q n species in alkali silicate glasses. J Am Ceram Soc 103(7):3991–4001
21. González-Henríquez CM, Terraza Claudio A, Sarabia M (2014) Theoretical and experimental vibrational spectroscopic investigation of two R1R2-diphenylsilyl-containing monomers and their optically active derivative polymer. J Phys Chem A 118(7):1175–1184
22. Oliver WC, Pharr GM (1992) An improved technique for determining hardness and elastic modulus using load and displacement sensing indentation experiments. J Mater Res 7(6):1564–1583